

# Electronic Character of Charge Order in Square-Planar Low-Valence Nickelates

Y. Shen<sup>1,\*</sup>, J. Sears<sup>1</sup>, G. Fabbris<sup>2</sup>, J. Li<sup>3</sup>, J. Pellicciari<sup>3</sup>, M. Mitrano<sup>4</sup>, W. He<sup>1</sup>, Junjie Zhang<sup>5,6</sup>, J. F. Mitchell<sup>5</sup>,  
V. Bisogni<sup>3</sup>, M. R. Norman<sup>5</sup>, S. Johnston<sup>7,8</sup> and M. P. M. Dean<sup>1,7,†</sup>

<sup>1</sup>Condensed Matter Physics and Materials Science Department,  
Brookhaven National Laboratory, Upton, New York 11973, USA

<sup>2</sup>Advanced Photon Source, Argonne National Laboratory, Lemont, Illinois 60439, USA

<sup>3</sup>National Synchrotron Light Source II, Brookhaven National Laboratory, Upton, New York 11973, USA


<sup>4</sup>Department of Physics, Harvard University, Cambridge, Massachusetts 02138, USA

<sup>5</sup>Materials Science Division, Argonne National Laboratory, Lemont, Illinois 60439, USA

<sup>6</sup>Institute of Crystal Materials, Shandong University, Jinan, Shandong 250100, China

<sup>7</sup>Department of Physics and Astronomy, The University of Tennessee, Knoxville, Tennessee 37966, USA

<sup>8</sup>Institute of Advanced Materials and Manufacturing, The University of Tennessee,  
Knoxville, Tennessee 37996, USA

 (Received 19 August 2022; revised 20 December 2022; accepted 10 January 2023; published 21 February 2023)

Charge order is a central feature of the physics of cuprate superconductors and is known to arise from a modulation of holes with primarily oxygen character. Low-valence nickelate superconductors also host charge order, but the electronic character of this symmetry breaking is unsettled. Here, using resonant inelastic x-ray scattering at the Ni  $L_2$  edge, we identify intertwined involvements of Ni  $3d_{x^2-y^2}$ ,  $3d_{3z^2-r^2}$ , and O  $2p_\sigma$  orbitals in the formation of diagonal charge order in an overdoped low-valence nickelate  $\text{La}_4\text{Ni}_3\text{O}_8$ . The Ni  $3d_{x^2-y^2}$  orbitals, strongly hybridized with planar O  $2p_\sigma$ , largely shape the spatial charge distribution and lead to Ni site-centered charge order. The  $3d_{3z^2-r^2}$  orbitals play a small, but non-negligible role in the charge order as they hybridize with the rare-earth  $5d$  orbitals. Our results reveal that the low-energy physics and ground-state character of these nickelates are more complex than those in cuprates.

DOI: [10.1103/PhysRevX.13.011021](https://doi.org/10.1103/PhysRevX.13.011021)

Subject Areas: Condensed Matter Physics

## I. INTRODUCTION

One of the common threads linking different classes of unconventional superconductors is their propensity to host proximate competing orders such as charge and spin stripes [1,2]. For example, the cuprate superconductors exhibit diagonal (with respect to the Cu—O bonds) spin stripes when underdoped [3–5], while Cu—O bond-oriented (parallel) charge order dominates the rest of the phase diagram [6,7]. The detection of superconductivity and charge order in the square-planar low-valence family of nickelates therefore presents a fascinating opportunity to study the degree of similarity between different unconventional superconducting families [8–17]. Intriguingly, different nickelates within the structural series of  $R_{n+1}\text{Ni}_n\text{O}_{2n+2}$  ( $R$  stands for a rare earth and  $n$  is the number of neighboring  $\text{NiO}_2$  layers) also host different charge ordered

phases. Underdoped materials with  $n = \infty$  and  $R = \text{La, Nd}$  exhibit parallel charge order [15–17], whereas  $n = 3$  material  $\text{La}_4\text{Ni}_3\text{O}_8$ , which is effectively 1/3 overdoped, manifests diagonal charge order [14]. Many researchers have emphasized that charge order plays an important role in the physics of cuprates [18–21]. In particular, there is good evidence showing that charge and spin order are a fundamental feature of minimal Hubbard model descriptions of the cuprates [22–24]. Some researchers have suggested that charge and spin order can intertwine with superconductivity to form pair density waves [25,26], or that dynamic charge or spin fluctuations might promote superconductivity [27–29]. Others have associated charge order fluctuations with the anomalous “strange metal” electronic transport in cuprates [30]. Understanding the electronic states involved in charge order formation is a prerequisite to testing all these scenarios in low-valence nickelates and is also important more generally for understanding charge order as a prevalent feature of correlated quantum materials.

Here, we use Ni  $L_2$ -edge resonant inelastic x-ray scattering (RIXS) to determine the electronic character of the charge order in  $\text{La}_4\text{Ni}_3\text{O}_8$ . We find that both the Ni  $3d_{x^2-y^2}$  and  $3d_{3z^2-r^2}$  orbitals are involved in charge order formation. The former contributes most of the charge modulation while

\*yshen@bnl.gov

†mdean@bnl.gov

Published by the American Physical Society under the terms of the [Creative Commons Attribution 4.0 International license](https://creativecommons.org/licenses/by/4.0/). Further distribution of this work must maintain attribution to the author(s) and the published article's title, journal citation, and DOI.

the latter dominates the RIXS spectra in the postedge regime and so plays a less important role. As the charge-transfer energy of these nickelates is larger than that of cuprates but comparable to the on-site Coulomb interaction, the holes involved in the charge modulation reside predominately on Ni sites, despite an appreciable amount of holes occupying the O orbitals. Our results indicate that the low-energy electronic structure and charge order of low-valence nickelates is largely shaped by hybridized  $3d_{x^2-y^2}$  and planar O  $2p_\sigma$  orbitals, similar to cuprates, while some differences exist due to the multiband physics introduced by Ni  $3d_{3z^2-r^2}$  orbitals hybridized with rare-earth  $5d$  states.

## II. RESULTS

The  $\text{La}_4\text{Ni}_3\text{O}_8$  nickelate samples studied here were prepared by reducing single crystals synthesized via the floating zone method (see Appendix A for details), and will be indexed in terms of scattering vector  $\mathbf{Q}$  in units of  $(2\pi/a, 2\pi/a, 2\pi/c)$  with  $a = b = 3.97 \text{ \AA}$ ,  $c = 26.092 \text{ \AA}$ . As the  $n = 3$  member of the low-valence nickelate family,  $\text{La}_4\text{Ni}_3\text{O}_8$  possesses a trilayer structure with a nominal  $3d^{8+2/3}$  valence. This leads to a  $1/3$ -hole self-doping with respect to the undoped  $3d^9$  state, putting it in the overdoped regime of the phase diagram [13,31]. It shares the same structural motif as infinite-layer nickelates with

square-planar  $\text{NiO}_2$  layers stacked without apical oxygens, leading to dominant Ni  $3d_{x^2-y^2}$  character near the Fermi energy. Although  $\text{La}_4\text{Ni}_3\text{O}_8$  has two inequivalent  $\text{NiO}_2$  layers, they are expected to show similar electronic structure as indicated by theoretical calculations [32,33], which is further supported by the observation that the same charge order pattern is formed in both types of layers [14]. We study their properties using Ni  $L_2$ -edge RIXS in order to avoid interference from the La  $M_4$  edge, which overlaps with the Ni  $L_3$  edge (see Appendix B for details). As shown in Fig. 1(a), charge order in  $\text{La}_4\text{Ni}_3\text{O}_8$  is quasi-two-dimensional in nature and occurs at the charge order (CO) wavevector  $\mathbf{Q}_\parallel = \mathbf{Q}_{\text{CO}} = (1/3, 1/3)$ , where a strong peak is observed in the quasielastic region of the RIXS intensity map at 40 K [see Fig. 1(b)]. The in-plane correlation length is larger than 100 nm, which might be limited by the sample mosaic, suggesting the long-range nature of the charge order [14]. This charge order peak persists up to 90 K and disappears above 110 K, indicating a transition temperature of around 100 K [see Figs. 1(c)–1(h)], consistent with the reported charge order from hard x-ray diffraction measurements [14]. No indication of charge order is apparent in equivalent measurements of metallic  $\text{Pr}_4\text{Ni}_3\text{O}_8$  samples prepared in the same way (see Supplemental Material Sec. I [34]).

We begin by identifying the active electronic states in  $\text{La}_4\text{Ni}_3\text{O}_8$  using x-ray spectroscopy. Figures 2(a) and 2(b)

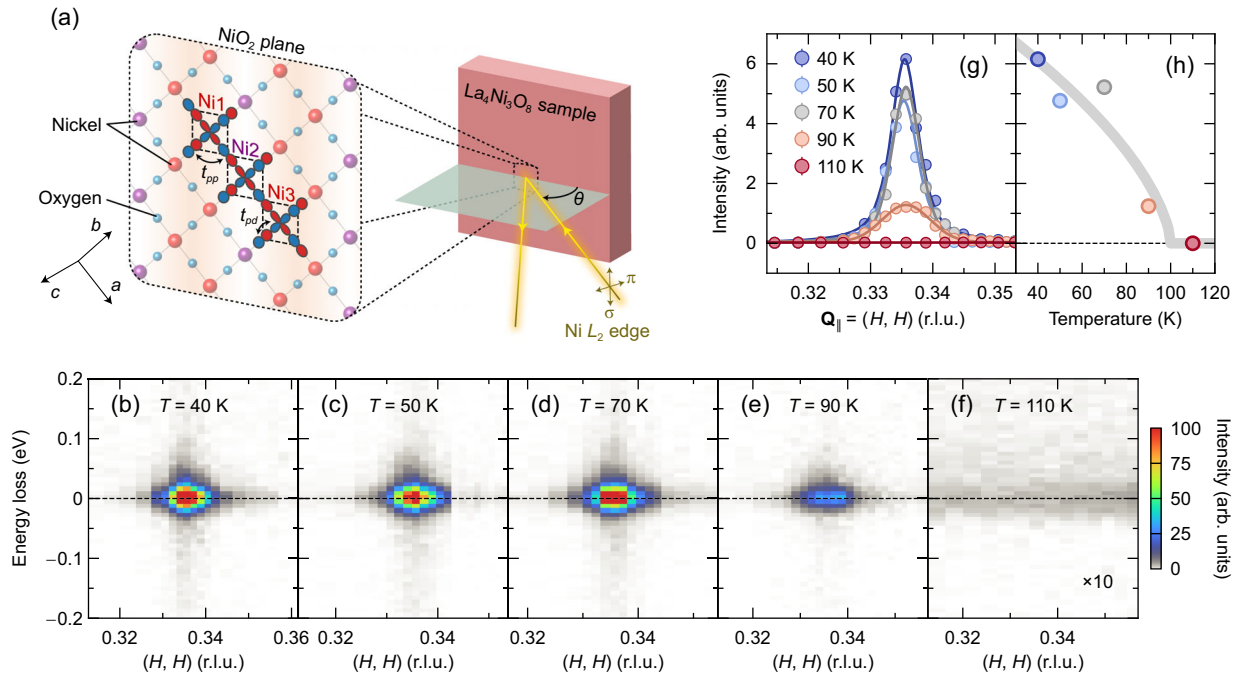


FIG. 1. Charge order transition in  $\text{La}_4\text{Ni}_3\text{O}_8$ . (a) Schematic of the Ni  $L_2$ -edge RIXS experimental setup. A single  $\text{NiO}_2$  layer is presented with stripes running vertically. A  $\text{Ni}_3\text{O}_{10}$  cluster composed of Ni  $3d_{x^2-y^2}$  and planar O  $2p_\sigma$  orbitals is embedded in it, tracing the charge order motif, in which hole poor Ni1 and Ni3 sites, shown in red, flank the hole rich Ni2 site depicted in purple. (b)–(f) RIXS intensity maps with  $\sigma$  polarized incident photons at the indicated temperatures obtained by changing the in-plane sample angle  $\theta$ . (g) Quasi-elastic-line amplitudes extracted from the data presented in (b)–(f) as a function of in-plane momentum transfer in reciprocal lattice units (r.l.u.). The solid lines are fitting curves with pseudo-Voigt profiles. (h) Temperature dependence of the fitted peak amplitudes. The bold gray line is a guide to the eye.

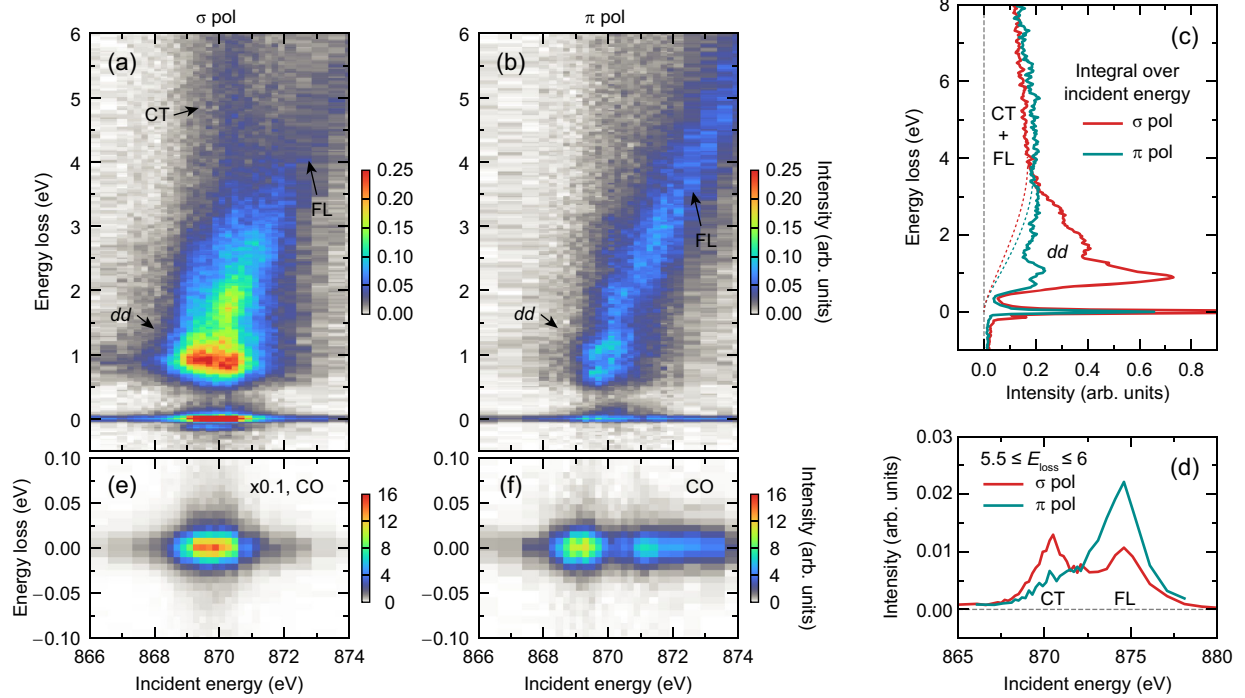


FIG. 2. RIXS energy maps and the resonant behaviors of the charge order (CO) peak. (a),(b) RIXS intensity maps as a function of incident photon energy with (a)  $\sigma$  x-ray polarization in the  $ab$  plane of the sample and (b)  $\pi$  x-ray polarization approximately parallel to the  $c$  axis. Several components can be identified: charge-transfer excitations (CT),  $dd$  excitations ( $dd$ ), and constant-emission-energy fluorescence (FL). (c) Integral of the RIXS spectra along the incident energy axis. The dashed lines are guides to the eye. (d) Incident energy dependence of the integrated RIXS spectra between 5.5 and 6 eV energy loss. (e),(f) RIXS intensity maps around the quasielastic regime with  $Q$  fixed at  $Q_{CO}$ . Note that the intensity in (e) is multiplied by 0.1 for clarity in visualizing the signal.

show the  $L_2$ -edge RIXS energy maps taken with  $\sigma$  x-ray polarization in the  $ab$  plane and  $\pi$  x-ray polarization approximately parallel to the  $c$  axis, respectively. The RIXS maps mainly comprise  $dd$  and charge-transfer excitations that are predominantly localized and resonate at the Ni  $L_2$  edge, and diagonal fluorescence features (see Supplemental Material Sec. II [34]). To distinguish among these contributions, we integrated the RIXS spectra along the incident energy axis and show the result in Fig. 2(c). With  $\sigma$  polarization, the spectra above 4 eV energy loss are dominated by mostly featureless fluorescence originating from particle-hole excitations that can be understood from an itinerant framework involving transitions from extended electronic bands spanning many unit cells [38]. Charge-transfer excitations are also visible above 4 eV but only at resonance. Below 4 eV, prominent  $dd$  excitations emerge that dominate over the featureless fluorescence (dashed lines). With  $\pi$  polarization, the fluorescence contributes most of the spectral weight and the  $dd$  excitations are much weaker. The strong dichroism of  $dd$  excitations reflects the dominant Ni  $3d_{x^2-y^2}$  orbital character near the Fermi energy in low-valence nickelates.

To further distinguish between charge-transfer excitations and fluorescence, we inspect the RIXS spectra between 5.5 and 6 eV energy loss, well above the  $dd$  excitation threshold. As shown in Fig. 2(d), the charge-

transfer excitations and fluorescence are separated in the incident energy axis, with the former stronger in the  $\sigma$  polarization channel, indicating appreciable  $d_{x^2-y^2}$ - $p_\sigma$  hybridization where  $p_\sigma$  indicates O orbitals that are parallel to the Ni—O bonds. In contrast, the fluorescence is stronger in the  $\pi$  polarization channel, suggesting that states involving Ni  $3d_{3z^2-r^2}$  orbitals dominate the fluorescence for a broad range of energy losses above  $\sim 3$  eV. The broadness of these states is in contrast with cuprates, and suggests that although the Ni  $3d_{3z^2-r^2}$  orbitals are mostly occupied and localized, their unoccupied components are hybridized with the rare-earth  $5d$  orbitals and thus contribute to dispersive states. This conclusion is consistent with combined density functional plus dynamical mean field theory (DFT+DMFT) calculations [32], as well as DFT+DMFT-based RIXS simulations for  $RNiO_2$  that studied the effect of switching on and off the rare-earth hybridization [39]. Meanwhile, the Ni  $3d_{x^2-y^2}$  orbitals exhibit less hybridization with the rare-earth  $5d$  orbitals and are more localized. Here, since we are measuring at the Ni  $L$  edge and the Ni  $t_{2g}$  orbitals are expected to lie well below the Fermi energy, we only consider Ni  $e_g$  orbitals [34].

Based on the resonant behavior of the different states identified, we now examine how the  $3d_{x^2-y^2}$  and  $3d_{3z^2-r^2}$  orbitals participate in the charge order. Figures 2(e) and 2(f)

show the RIXS energy maps around the quasielastic regime at  $\mathbf{Q}_{\text{CO}}$ , i.e. the resonant elastic x-ray scattering (REXS) signals. The peak intensity strongly resonates at the Ni  $L_2$  edge in the  $\sigma$  polarization channel [see Fig. 2(e)], confirming that the  $(1/3, 1/3)$  Bragg peak in  $\text{La}_4\text{Ni}_3\text{O}_8$  involves a charge modulation and is not purely structural. Surprisingly, the charge order peak in the  $\pi$  polarization channel, although much weaker, resonates at the preedge and postedge regimes but not at the main edge [see Fig. 2(f)], distinct from that in cuprates [40–42]. First, this observation indicates that both the  $3d_{x^2-y^2}$  and  $3d_{3z^2-r^2}$  orbitals are involved in charge order formation with the latter much less prominent. Second, the charge order peak in the postedge regime with  $\pi$  polarization suggests that the states far above the Fermi energy also show charge modulation, which is mostly contributed by  $3d_{3z^2-r^2}$  orbitals. Considering that the  $3d_{3z^2-r^2}$  density of states in the postedge regime is likely caused by hybridization with the rare-earth  $5d$  orbitals, this indicates potential involvement of rare-earth orbitals in the charge order formation. Similarly, the weak preedge charge order peak with  $\pi$  polarization indicates that the  $3d_{3z^2-r^2}$  density of states near the Fermi energy is nonzero but small.

Having established the involvement of Ni orbitals in the charge order formation, now we look at the role of oxygen states. To do this, we use exact diagonalization methods which allow us to solve the resonant cross section and break down the contributions from different states. Since the charge order is commensurate with a period of three Ni sites and there is a strong hybridization between the Ni and O orbitals, the smallest cluster one can use to describe the charge ordered state involves three Ni-O plaquettes, which we label 1, 2, and 3. We choose a bond-oriented cluster, as illustrated in Fig. 1(a), given that the Ni-O hopping dominates the kinetic energy. In order to compute REXS, we use the atomic scattering factors from the cluster and add these amplitudes to simulate an effective two-dimensional  $\text{NiO}_2$  plane as shown in Fig. 1(a). The appropriate parameters for this cluster, and in particular the charge-transfer energy  $\Delta = 5.6$  eV and the on-site Coulomb repulsion  $U_{dd} = 6.5$  eV, have been empirically determined by prior x-ray measurements of this material at the O  $K$  edge [43]. We use open boundary conditions and construct the Hamiltonian in the hole language (see Appendix C for details). Four holes are introduced to the cluster, which is appropriate for the  $d^{9-1/3}$  electronic configuration of  $\text{La}_4\text{Ni}_3\text{O}_8$ . Without any additional constraints, the holes will be evenly distributed among different  $\text{NiO}_4$  plaquettes with minimal charge disproportionation and no symmetry breaking is expected. To realize the charge order observed in  $\text{La}_4\text{Ni}_3\text{O}_8$ , we manually introduce a potential difference [44],  $\Delta\epsilon_d$ , for different Ni sites by lowering the orbital energies of Ni2 by  $2\Delta\epsilon_d/3$  and raising those of Ni1 and Ni3 by  $\Delta\epsilon_d/3$ . Based on the similar magnetic exchange of charge ordered  $\text{La}_4\text{Ni}_3\text{O}_8$  and

metallic  $\text{Pr}_4\text{Ni}_3\text{O}_8$  [45],  $\Delta\epsilon_d$  must be significantly smaller than the charge-transfer energy. Thus, we choose it to be  $\Delta\epsilon_d = 0.8$  eV while noting that apart from modulating the intensity of the charge order peak, the results are similar provided  $\Delta\epsilon_d$  is not made unfeasibly large (see Supplemental Material Fig. S5 [34]). This choice leads to a charge disproportionation of  $\Delta n = 0.32$ , which is of a similar order of magnitude as that in cuprates [40]. This value is much smaller than the fully disproportionated limit  $\Delta n = 1$ , consistent with density functional theory calculations that indicate a small charge modulation upon charge ordering in this system [31]. When examining the electronic configuration of the cluster, we find that the ground state is a singlet, and the first excited state is a triplet, which is around 70 meV above the ground state, consistent with the magnetic excitations found in  $\text{La}_4\text{Ni}_3\text{O}_8$  [45].

Figure 3 shows the calculated Ni  $L_2$ -edge RIXS energy maps with all the Ni  $3d$  and O  $2p$  orbitals included, which qualitatively reproduce the localized  $dd$  excitations observed experimentally. Note that the small cluster size means that we can only capture a limited number of discrete states. For this reason, fluorescence features are not fully captured, which would require a continuous distribution of states. This can be seen more clearly in the  $\pi$  polarization channel where the fluorescence dominates the spectra in experimental data [see Fig. 2(b)], but only the weak  $dd$  excitations are present in our cluster calculations [see Fig. 3(b)].

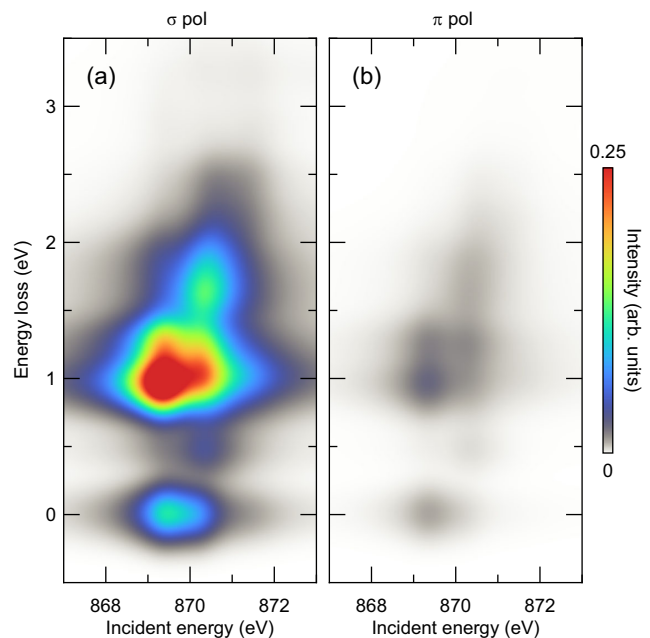


FIG. 3. Low-energy electronic states in  $\text{La}_4\text{Ni}_3\text{O}_8$ . Calculations of the RIXS energy maps at the Ni  $L_2$  edge for (a)  $\sigma$  and (b)  $\pi$  incident x-ray polarization. The calculations reproduce the experimental energy scale and polarization of the  $dd$  excitations, evincing an appropriate minimal model for  $\text{La}_4\text{Ni}_3\text{O}_8$ .

Having verified the relevant parameters via the RIXS maps, we computed the x-ray absorption spectrum (XAS) and REXS response of  $\text{La}_4\text{Ni}_3\text{O}_8$  using a similar exact diagonalization approach and identical parameters and plot the results in Fig. 4 (see Supplemental Material Sec. V [34]). The charge disproportionation in the cluster implies a REXS response at  $\mathbf{Q}_{\text{CO}}$ . The predicted REXS resonance shown in Fig. 4(c) nicely captures the main two peak structure of the experimental REXS resonance shown in Fig. 4(b). The same applies for the XAS as shown in Fig. 4(a). In fact, the line shape of the resonant profile of the

charge order peak is sensitive to the charge-transfer energy, and neither the pure charge transfer nor Mott-Hubbard scenarios can describe the observed resonant behaviors (see Supplemental Material Fig. S6 [34]), demonstrating the mixed charge-transfer—Mott-Hubbard characters of charge order in this material. To understand the nature of the two resonant features, we projected the wave functions of the RIXS intermediate states onto the Fock basis which specifies the location of the holes. Two main manifolds are seen for each Ni site. The first manifold is primarily attributed to transitions resonant with  $d^{10}\underline{L}^0$  states, where  $\underline{L}$  stands for ligand holes on the four oxygen  $\sigma$  orbitals surrounding the Ni site. The second manifold is mainly resonant with  $d^9\underline{L}^0$  and  $d^{10}\underline{L}^1$  states caused by the doped holes, similar to the cuprates [46,47]. With nonzero  $\Delta\epsilon_d$ , the manifolds of different Ni sites split along the incident energy axis, as shown in Fig. 4(c). The successful description of the charge order in  $\text{La}_4\text{Ni}_3\text{O}_8$  using our cluster model indicates that about 70% of the holes participating in the charge modulation are on Ni, with the remaining 30% on oxygen, as depicted in the inset of Fig. 4(b).

### III. DISCUSSION

Our Ni-dominant charge order distribution is quite different from cuprates, in which the charge order has dominant oxygen character [40,48]. This difference mainly arises from the larger charge-transfer energy in nickelates compared to cuprates. Another difference is that in cuprates, the  $3d_{3z^2-r^2}$  orbitals are strongly localized at energies more than 1.5 eV away from the  $3d_{x^2-y^2}$  orbitals [49], and thus not involved in the low-energy physics. For square-planar nickelates, our analysis of  $\text{La}_4\text{Ni}_3\text{O}_8$  indicates that the  $3d_{3z^2-r^2}$  density of states, though small, is spread out over an extended energy range, likely due to hybridization with the rare-earth  $5d$  orbitals. It should be noted that although the  $3d_{3z^2-r^2}$  orbital involvement in the charge order formation is nonzero, its contribution is much less than the hybridized  $3d_{x^2-y^2}$  and  $2p_\sigma$  orbitals, as indicated by the stronger charge order peak in the  $\sigma$  polarization channel. These factors mean that minimal theoretical models of charge order in nickelates must explicitly include both Ni and O states alongside strong correlations. Another result of our model is that the doped sites in charge ordered nickelates are much closer to a low-spin  $S = 0$  state than to a high-spin  $S = 1$  state, unlike  $\text{La}_{2-x}\text{Sr}_x\text{NiO}_4$ , whose high-spin physics drives insulating behavior across the vast majority of its phase diagram [50].

Recently, RIXS measurements in infinite-layer nickelate films have discovered and studied charge order at  $\mathbf{Q}_{\parallel} = (1/3, 0)$  in undoped and underdoped samples [15–17], resembling the charge order in cuprates, but differing from the diagonal charge order in  $\text{La}_4\text{Ni}_3\text{O}_8$ . In terms of these differing wave vectors, theoretical model studies in the cuprates have shown that charge order at  $(Q, 0)$  and  $(Q, Q)$  are close in energy, the eventual choice of the charge order

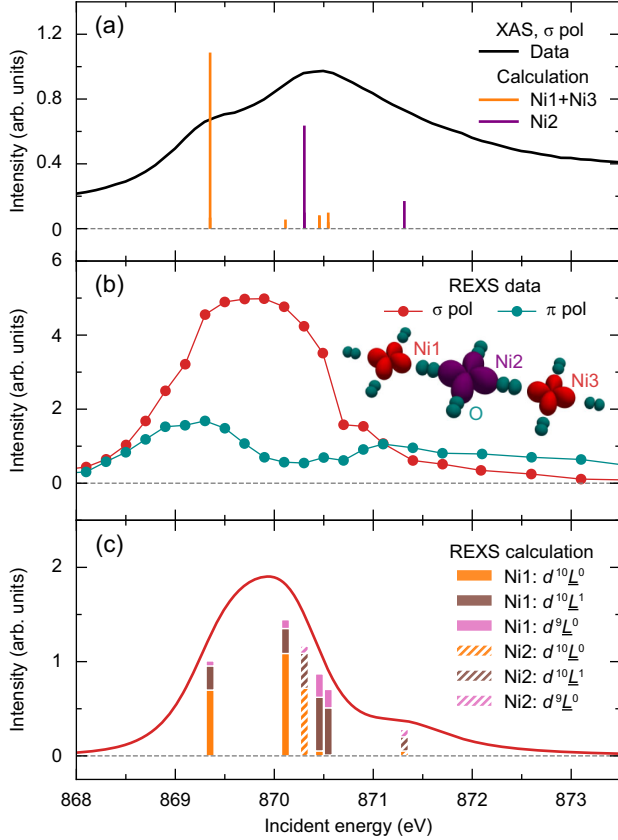


FIG. 4. Electronic character of charge order. (a) X-ray absorption spectrum (XAS) data at the Ni  $L_2$  edge in the  $\sigma$  polarization channel along with the calculation results with  $\Delta\epsilon_d = 0.8$  eV. Note that Ni1 and Ni3 are symmetry related. (b) Fitted peak amplitudes of the quasielastic intensities presented in Figs. 2(e) and 2(f), representing the resonant behaviors of the charge order peak. Inset: schematic of the electronic character of the charge order, showing a dominant modulation of Ni orbitals along with an appreciable modulation of the oxygen orbitals. (c) Simulation of the incident energy dependence of the charge order peak intensity with  $\sigma$  incident polarization and  $\Delta\epsilon_d = 0.8$  eV. The vertical bars are weights of different configurations of the RIXS intermediate states, the total height of which is normalized according to the simulated charge order peak intensity of each state. The accurate simulation of the Ni  $3d$  and O  $2p$  components of the resonance verifies our model, which is used to extract the electronic character of the charge order illustrated in the inset of (b).

wave vector being sensitive to details of the electronic structure and correlations [51,52]. This idea is supported by the experimental observation that the doping dependent charge order wave vector varies in different cuprate families [20], similar to what has been seen more recently in the infinite-layer nickelates [15]. In view of this, the difference in wave vector probably does not reflect a difference in the mechanisms at play in charge order formation. It should, however, be noted that the parallel charge order seen in infinite-layer materials occurs at a lower hole concentration.

More information can be obtained by comparing the states involved in charge order formation for different low-valence nickelates [15–17]. All these recent works support an appreciable role for Ni in charge order formation. However, controversy exists regarding whether the rare-earth-Ni hybridization is crucial for charge order formation [16], or whether the charge modulation on rare-earth states only plays a secondary parasitic role [15]. Our results support the latter scenario in  $\text{La}_4\text{Ni}_3\text{O}_8$ . Regarding the involvement of oxygen states, we provide the first spectroscopic modeling that allows this question to be addressed quantitatively. We deduce a mixed charge-transfer—Mott-Hubbard picture for the charge order and 70%/30% split of Ni versus O contributions to the charge modulation. This contradicts some of the previous suggestions for infinite-layer nickelates, which propose a negligible role for oxygen in charge order formation and that in-plane and out-of-plane Ni states contribute roughly equally [16]. These differences are puzzling considering that different members of the  $R_{n+1}\text{Ni}_n\text{O}_{2n+2}$  family share similar Ni—O bonding, magnetic exchange [45,53], superconducting transition temperatures [12,13,54,55], and calculated electronic structures [56]. Part of the challenge of making this comparison is that RIXS maps of infinite-layer films, as well as their charge order properties, vary substantially between different samples of nominally the same composition [15–17]. In this regard, our quantitative spectroscopic analysis on single crystals is valuable considering that these samples show more consistent spectral properties than films of infinite-layer materials [15–17].

#### IV. CONCLUSION

In summary, we have used RIXS measurements at the Ni  $L_2$  edge to study the character of the electronic structure and charge order in the low-valence nickelate  $\text{La}_4\text{Ni}_3\text{O}_8$ . Our work is unique in providing a realistic quantitative empirical model for charge order and validating it using  $\mathbf{Q}$ -resolved spectroscopy at the charge order wave vector. Different from cuprates where the spatial charge modulation dominantly resides on ligand orbitals, the charge order in  $\text{La}_4\text{Ni}_3\text{O}_8$  is mostly contributed by the Ni sites due to the larger charge-transfer energy in low-valence nickelates. In addition to the dominant role of in-plane Ni  $3d_{x^2-y^2}$  and O  $2p_\sigma$  orbitals, the out-of-plane Ni  $3d_{3z^2-r^2}$  orbitals also participate in the charge order, this being enabled by their

hybridization with the rare-earth  $5d$  orbitals. Thus, our results reveal that the overall low-energy physical properties of low-valence nickelates are shaped by Ni  $3d_{x^2-y^2}$  and O  $2p_\sigma$  orbitals, while the detailed electronic structure is fine-tuned by Ni  $3d_{3z^2-r^2}$  and rare-earth  $5d$  orbitals. This reveals that multiorbital physics is crucial to low-valence nickelates, indicating that several different ground states are close in energy. This observation points to a more complex, and perhaps an even richer, phenomenology than their cuprate cousins, while charge order remains an intrinsic character of these strongly correlated materials.

The RIXS data generated in this study have been deposited in the Zenodo database [61].

#### ACKNOWLEDGMENTS

Work at Brookhaven and the University of Tennessee (RIXS measurements and the interpretation and model Hamiltonian calculations) was supported by the U.S. Department of Energy, Office of Science, Office of Basic Energy Sciences, under Award No. DE-SC0022311. Work at Argonne was supported by the U.S. DOE, Office of Science, Basic Energy Sciences, Materials Science and Engineering Division (nickelate sample synthesis and first principles calculations). Work performed at Harvard University (data interpretation and paper writing) was supported by the U.S. Department of Energy, Division of Materials Science, under Contract No. DE-SC0012704. This research used resources at the SIX beam line of the National Synchrotron Light Source II, a U.S. DOE Office of Science User Facility operated for the DOE Office of Science by Brookhaven National Laboratory under Contract No. DE-SC0012704. This research used resources of the Advanced Photon Source, a U.S. Department of Energy (DOE) Office of Science user facility at Argonne National Laboratory and is based on research supported by the U.S. DOE Office of Science-Basic Energy Sciences, under Contract No. DE-AC02-06CH11357.

#### APPENDIX A: SAMPLE SYNTHESIS

Parent Ruddlesden-Popper  $\text{La}_4\text{Ni}_3\text{O}_{10}$  and  $\text{Pr}_4\text{Ni}_3\text{O}_{10}$  were prepared using the high-pressure optical floating zone method. Sample reduction was performed by cleaving small crystals from the boules and heating them in a flowing  $\text{H}_2/\text{Ar}$  gas mixture as described previously [31]. We adopt the tetragonal notation with space group  $I4/mmm$  and lattice constants of  $a = b = 3.97 \text{ \AA}$ ,  $c = 26.092 \text{ \AA}$  to describe reciprocal space. Using this notation, the samples had a  $c$ -axis surface normal. The high quality of these samples is confirmed by prior studies [43,45]. Single crystals of  $\text{La}_4\text{Ni}_3\text{O}_8$  are particularly suitable for this study as they exhibit more consistent XAS spectra and charge order properties than thin films of infinite-layer nickelates [15–17].

## APPENDIX B: RIXS MEASUREMENTS

High-energy-resolution RIXS measurements were performed at the SIX beam line at the NSLS-II. Although the sample geometry and the energy of the Ni  $L_2$ -edge resonance limits reciprocal space access, charge order in  $\text{La}_4\text{Ni}_3\text{O}_8$  has a  $c$ -axis correlation length of less than one unit cell, which means that the charge order Bragg peaks are accessible for a wide range of  $L$  values [14]. We chose to measure at the Ni  $L_2$  edge instead of the  $L_3$  edge to avoid contamination from the La  $M$  edge which is very close to the Ni  $L_3$  edge and can strongly distort the resonant process [58]. In view of this, we fixed the spectrometer angle at its maximum value of  $2\Theta = 153^\circ$  throughout the measurements of the charge order peak. The samples were aligned with the crystalline  $[0, 0, L]$  and  $[H, H, 0]$  directions lying in the horizontal scattering plane to access the charge order peak with momentum transfer  $\mathbf{Q}_{\text{CO}} = (1/3, 1/3, L)$ , where  $L \approx 1.75$ . In this geometry, the x-ray intensity is dominated by charge, rather than spin, scattering (see Supplemental Material Sec. IV [34]). Spectra designed to study the charge order resonance in the  $\sigma$  polarization channel, such as Fig. 2(e), were taken with 24 meV energy resolution. For the charge order in the  $\pi$  polarization channel, such as Fig. 2(f), a relaxed energy resolution of 32 meV was used to increase throughput. Whenever the energy was changed, the sample was rotated in order to remain at the same in-plane scattering vector. In order to study the high-energy features, as done in Figs. 2(a) and 2(b), the energy resolution was further relaxed to 48 meV and the sample and spectrometer were slightly offset from the diffraction condition with a sample angle of  $14.3^\circ$  and a spectrometer angle of  $2\Theta = 147^\circ$  to avoid saturating the detector. Note that the strong elastic intensity overwhelms the low-energy inelastic signals such as that from the magnetic excitations studied previously [45]. Data collected with different energy-resolution configurations were normalized by the  $dd$  excitations measured with the same sample geometry.

Upon illumination by very strong elastic scattering from charge order, a weak periodic error was identified in the spectrometer grating which created the weak feature in the energy gain side of Fig. 2(a). This was confirmed by measuring reference elastic scattering.

## APPENDIX C: EXACT DIAGONALIZATION CALCULATIONS

The RIXS spectra and REXS responses presented here were calculated using the Kramers-Heisenberg formula in the dipole approximation through the EDRIXS software [59,60]. The eigenstates for the initial, final, and intermediate states are obtained from exact diagonalization of a  $\text{Ni}_3\text{O}_{10}$  cluster with four holes and open boundary conditions. To fully take into account the many-body and multiorbital effects, we explicitly include the Coulomb interactions and nearest-neighbor interatomic hoppings in

our model, and construct the Hamiltonian in hole language. We use the same parameters as those used in the O  $K$ -edge calculations which are proved to well describe the RIXS data [43]. By doing so, the charge-transfer energy  $\Delta$  is set to 5.6 eV and the on-site Coulomb repulsion to 6.5 eV, locating the material in the mixed charge-transfer—Mott-Hubbard regime of the Zaanen-Sawatzky-Allen scheme. We also include the spin-orbit coupling for the Ni 3d electrons, which is very small and is expected to play a minimal role. For simplicity, the scattering angle  $2\Theta$  is kept at  $150^\circ$  and the sample angle is fixed to  $\theta = 15^\circ$ .

The total RIXS scattering amplitude is calculated via

$$\mathcal{F} = \sum_i \mathcal{F}_i e^{i\mathbf{Q}\cdot\mathbf{r}_i}, \quad (\text{C1})$$

where  $\mathcal{F}_i$  and  $\mathbf{r}_i$  are the scattering amplitude and position of each Ni site, respectively. The charge order peak was then calculated by combining the atomic scattering amplitudes with the phases appropriate for tiling the cluster into the  $\text{NiO}_2$  plane as shown in Fig. 1(a).

- 
- [1] M. R. Norman, *The Challenge of Unconventional Superconductivity*, *Science* **332**, 196 (2011).
  - [2] D. J. Scalapino, *A Common Thread: The Pairing Interaction for Unconventional Superconductors*, *Rev. Mod. Phys.* **84**, 1383 (2012).
  - [3] K. Yamada, C. H. Lee, K. Kurahashi, J. Wada, S. Wakimoto, S. Ueki, H. Kimura, Y. Endoh, S. Hosoya, G. Shirane, R. J. Birgeneau, M. Greven, M. A. Kastner, and Y. J. Kim, *Doping Dependence of the Spatially Modulated Dynamical Spin Correlations and the Superconducting-Transition Temperature in  $\text{La}_{2-x}\text{Sr}_x\text{CuO}_4$* , *Phys. Rev. B* **57**, 6165 (1998).
  - [4] S. Wakimoto, J. M. Tranquada, T. Ono, K. M. Kojima, S. Uchida, S. H. Lee, P. M. Gehring, and R. J. Birgeneau, *Diagonal Static Spin Correlation in the Low-Temperature Orthorhombic Pccn Phase of  $\text{La}_{1.55}\text{Nd}_{0.4}\text{Sr}_{0.05}\text{CuO}_4$* , *Phys. Rev. B* **64**, 174505 (2001).
  - [5] S. R. Dunsiger, Y. Zhao, Z. Yamani, W. J. L. Buyers, H. A. Dabkowska, and B. D. Gaulin, *Incommensurate Spin Ordering and Fluctuations in Underdoped  $\text{La}_{2-x}\text{Ba}_x\text{CuO}_4$* , *Phys. Rev. B* **77**, 224410 (2008).
  - [6] R. Arpaia, S. Caprara, R. Fumagalli, G. De Vecchi, Y. Y. Peng, E. Andersson, D. Betto, G. M. De Luca, N. B. Brookes, F. Lombardi, M. Salluzzo, L. Braicovich, C. Di Castro, M. Grilli, and G. Ghiringhelli, *Dynamical Charge Density Fluctuations Pervading the Phase Diagram of a Cu-Based High- $T_c$  Superconductor*, *Science* **365**, 906 (2019).
  - [7] H. Miao, G. Fabbris, R. J. Koch, D. G. Mazzone, C. S. Nelson, R. Acevedo-Esteves, G. D. Gu, Y. Li, T. Yilmaz, K. Kaznatcheev, E. Vescovo, M. Oda, T. Kurosawa, N. Momono, T. Assefa, I. K. Robinson, E. S. Bozin, J. M. Tranquada, P. D. Johnson, and M. P. M. Dean, *Charge Density Waves in Cuprate Superconductors beyond the Critical Doping*, *npj Quantum Mater.* **6**, 31 (2021).
  - [8] D. Li, B. Y. Wang, K. Lee, S. P. Harvey, M. Osada, B. H. Goodge, L. F. Kourkoutis, and H. Y. Hwang,

- Superconducting Dome in Nd<sub>1-x</sub>Sr<sub>x</sub>NiO<sub>2</sub> Infinite Layer Films*, *Phys. Rev. Lett.* **125**, 027001 (2020).
- [9] S. Zeng, C. S. Tang, X. Yin, C. Li, M. Li, Z. Huang, J. Hu, W. Liu, G. J. Omar, H. Jani, Z. S. Lim, K. Han, D. Wan, P. Yang, S. J. Pennycook, A. T. S. Wee, and A. Ariando, *Phase Diagram and Superconducting Dome of Infinite-Layer Nd<sub>1-x</sub>Sr<sub>x</sub>NiO<sub>2</sub> Thin Films*, *Phys. Rev. Lett.* **125**, 147003 (2020).
- [10] M. Osada, B. Y. Wang, K. Lee, D. Li, and H. Y. Hwang, *Phase Diagram of Infinite Layer Praseodymium Nickelate Pr<sub>1-x</sub>Sr<sub>x</sub>NiO<sub>2</sub> Thin Films*, *Phys. Rev. Mater.* **4**, 121801(R) (2020).
- [11] M. Osada, B. Y. Wang, B. H. Goodge, S. P. Harvey, K. Lee, D. Li, L. F. Kourkoutis, and H. Y. Hwang, *Nickelate Superconductivity without Rare-Earth Magnetism: (La, Sr)NiO<sub>2</sub>*, *Adv. Mater.* **33**, 2104083 (2021).
- [12] S. Zeng, C. Li, E. Chow Lin, Y. Cao, Z. Zhang, S. Tang Chi, X. Yin, S. Lim Zhi, J. Hu, P. Yang, and A. Ariando, *Superconductivity in Infinite-Layer Nickelate La<sub>1-x</sub>Ca<sub>x</sub>NiO<sub>2</sub> Thin Films*, *Sci. Adv.* **8**, eabl9927 (2022).
- [13] G. A. Pan, D. Ferenc Segedin, H. LaBollita, Q. Song, E. M. Nica, B. H. Goodge, A. T. Pierce, S. Doyle, S. Novakov, D. Córdoba Carrizales *et al.*, *Superconductivity in a Quintuple-Layer Square-Planar Nickelate*, *Nat. Mater.* **21**, 160 (2022).
- [14] J. Zhang, Y.-S. Chen, D. Phelan, H. Zheng, M. R. Norman, and J. F. Mitchell, *Stacked Charge Stripes in the Quasi-2D Trilayer Nickelate La<sub>4</sub>Ni<sub>3</sub>O<sub>8</sub>*, *Proc. Natl. Acad. Sci. U.S.A.* **113**, 8945 (2016).
- [15] M. Rossi, M. Osada, J. Choi, S. Agrestini, D. Jost, Y. Lee, H. Lu, B. Y. Wang, K. Lee, A. Nag *et al.*, *A Broken Translational Symmetry State in an Infinite-Layer Nickelate*, *Nat. Phys.* **18**, 869 (2022).
- [16] C. C. Tam, J. Choi, X. Ding, S. Agrestini, A. Nag, B. Huang, H. Luo, M. García-Fernández, L. Qiao, and K.-J. Zhou, *Charge Density Waves in Infinite-Layer NdNiO<sub>2</sub> Nickelates*, *Nat. Mater.* **21**, 1116 (2022).
- [17] G. Krieger, L. Martinelli, S. Zeng, L. E. Chow, K. Kummer, R. Arpaia, M. Moretti Sala, N. B. Brookes, A. Ariando, N. Viart, M. Salluzzo, G. Ghiringhelli, and D. Preziosi, *Charge and Spin Order Dichotomy in NdNiO<sub>2</sub> Driven by the Capping Layer*, *Phys. Rev. Lett.* **129**, 027002 (2022).
- [18] J. M. Tranquada, *Spins, Stripes, and Superconductivity in Hole-Doped Cuprates*, *AIP Conf. Proc.* **1550**, 114 (2013).
- [19] R. Comin and A. Damascelli, *Resonant X-Ray Scattering Studies of Charge Order in Cuprates*, *Annu. Rev. Condens. Matter Phys.* **7**, 369 (2016).
- [20] A. Frano, S. Blanco-Canosa, B. Keimer, and R. J. Birgeneau, *Charge Ordering in Superconducting Copper Oxides*, *J. Phys. Condens. Matter* **32**, 374005 (2020).
- [21] J. M. Tranquada, M. P. M. Dean, and Q. Li, *Superconductivity from Charge Order in Cuprates*, *J. Phys. Soc. Jpn.* **90**, 111002 (2021).
- [22] E. W. Huang, C. B. Mendl, S. Liu, S. Johnston, H.-C. Jiang, B. Moritz, and T. P. Devereaux, *Numerical Evidence of Fluctuating Stripes in the Normal State of High-T<sub>c</sub> Cuprate Superconductors*, *Science* **358**, 1161 (2017).
- [23] B.-X. Zheng, C.-M. Chung, P. Corboz, G. Ehlers, M.-P. Qin, R. M. Noack, H. Shi, S. R. White, S. Zhang, and G. K.-L. Chan, *Stripe Order in the Underdoped Region of the Two-Dimensional Hubbard Model*, *Science* **358**, 1155 (2017).
- [24] P. Mai, S. Karakuzu, G. Balduzzi, S. Johnston, and T. A. Maier, *Intertwined Spin, Charge, and Pair Correlations in the Two-Dimensional Hubbard Model in the Thermodynamic Limit*, *Proc. Natl. Acad. Sci. U.S.A.* **119**, e2112806119 (2022).
- [25] Q. Li, M. Hücker, G. D. Gu, A. M. Tsvelik, and J. M. Tranquada, *Two-Dimensional Superconducting Fluctuations in Stripe-Ordered La<sub>1.875</sub>Ba<sub>0.125</sub>CuO<sub>4</sub>*, *Phys. Rev. Lett.* **99**, 067001 (2007).
- [26] E. Berg, E. Fradkin, E.-A. Kim, S. A. Kivelson, V. Oganesyan, J. M. Tranquada, and S. C. Zhang, *Dynamical Layer Decoupling in a Stripe-Ordered High-T<sub>c</sub> Superconductor*, *Phys. Rev. Lett.* **99**, 127003 (2007).
- [27] V. J. Emery, S. A. Kivelson, and O. Zachar, *Spin-Gap Proximity Effect Mechanism of High-Temperature Superconductivity*, *Phys. Rev. B* **56**, 6120 (1997).
- [28] S. A. Kivelson, E. Fradkin, and V. J. Emery, *Electronic Liquid-Crystal Phases of a Doped Mott Insulator*, *Nature (London)* **393**, 550 (1998).
- [29] E. Fradkin, S. A. Kivelson, and J. M. Tranquada, *Theory of Intertwined Orders in High Temperature Superconductors*, *Rev. Mod. Phys.* **87**, 457 (2015).
- [30] C. Castellani, C. Di Castro, and M. Grilli, *Singular Quasiparticle Scattering in the Proximity of Charge Instabilities*, *Phys. Rev. Lett.* **75**, 4650 (1995).
- [31] J. Zhang, A. Botana, J. Freeland, D. Phelan, H. Zheng, V. Pardo, M. Norman, and J. Mitchell, *Large Orbital Polarization in a Metallic Square-Planar Nickelate*, *Nat. Phys.* **13**, 864 (2017).
- [32] J. Karp, A. Hampel, M. Zingl, A. S. Botana, H. Park, M. R. Norman, and A. J. Millis, *Comparative Many-Body Study of Pr<sub>4</sub>Ni<sub>3</sub>O<sub>8</sub> and NdNiO<sub>2</sub>*, *Phys. Rev. B* **102**, 245130 (2020).
- [33] E. M. Nica, J. Krishna, R. Yu, Q. Si, A. S. Botana, and O. Erten, *Theoretical Investigation of Superconductivity in Trilayer Square-Planar Nickelates*, *Phys. Rev. B* **102**, 020504(R) (2020).
- [34] See Supplemental Material at <http://link.aps.org/supplemental/10.1103/PhysRevX.13.011021> for measurements of Pr<sub>4</sub>Ni<sub>3</sub>O<sub>8</sub>, discussion of the RIXS process, consideration of spin order, and further calculations, which includes Refs. [35–37].
- [35] M. W. Haverkort, M. Zwierzycki, and O. K. Andersen, *Multiplet Ligand-Field Theory Using Wannier Orbitals*, *Phys. Rev. B* **85**, 165113 (2012).
- [36] M. W. Haverkort, *Theory of Resonant Inelastic X-Ray Scattering by Collective Magnetic Excitations*, *Phys. Rev. Lett.* **105**, 167404 (2010).
- [37] A. J. Achkar, R. Sutarto, X. Mao, F. He, A. Frano, S. Blanco-Canosa, M. Le Tacon, G. Ghiringhelli, L. Braicovich, M. Minola, M. Moretti Sala, C. Mazzoli, R. Liang, D. A. Bonn, W. N. Hardy, B. Keimer, G. A. Sawatzky, and D. G. Hawthorn, *Distinct Charge Orders in the Planes and Chains of Ortho-III-Ordered YBa<sub>2</sub>Cu<sub>3</sub>O<sub>6+δ</sub> Superconductors Identified by Resonant Elastic X-Ray Scattering*, *Phys. Rev. Lett.* **109**, 167001 (2012).
- [38] G. Fabbri, D. Meyers, L. Xu, V. M. Katukuri, L. Hozoi, X. Liu, Z.-Y. Chen, J. Okamoto, T. Schmitt, A. Uldry, B. Delley,



- G. D. Gu, D. Prabhakaran, A. T. Boothroyd, J. van den Brink, D. J. Huang, and M. P. M. Dean, *Doping Dependence of Collective Spin and Orbital Excitations in the Spin-1 Quantum Antiferromagnet  $\text{La}_{2-x}\text{Sr}_x\text{NiO}_4$  Observed by X Rays*, *Phys. Rev. Lett.* **118**, 156402 (2017).
- [39] K. Higashi, M. Winder, J. Kuneš, and A. Hariki, *Core-Level X-Ray Spectroscopy of Infinite-Layer Nickelate: LDA + DMFT Study*, *Phys. Rev. X* **11**, 041009 (2021).
- [40] P. Abbamonte, A. Rusydi, S. Smađić, G. D. Gu, G. A. Sawatzky, and D. L. Feng, *Spatially Modulated “Mottness” in  $\text{La}_{2-x}\text{Ba}_x\text{CuO}_4$* , *Nat. Phys.* **1**, 155 (2005).
- [41] Y. Y. Peng, R. Fumagalli, Y. Ding, M. Minola, S. Caprara, D. Betto, M. Bluschke, G. M. De Luca, K. Kummer, E. Lefrançois, M. Salluzzo, H. Suzuki, M. Le Tacon, X. J. Zhou, N. B. Brookes, B. Keimer, L. Braicovich, M. Grilli, and G. Ghiringhelli, *Re-entrant Charge Order in Overdoped  $(\text{Bi}, \text{Pb})_{2.12}\text{Sr}_{1.88}\text{CuO}_{6+\delta}$  Outside the Pseudogap Regime*, *Nat. Mater.* **17**, 697 (2018).
- [42] J. Li, A. Nag, J. Pellicciari, H. Robarts, A. Walters, M. Garcia-Fernandez, H. Eisaki, D. Song, H. Ding, S. Johnston, R. Comin, and K.-J. Zhou, *Multiorbital Charge-Density Wave Excitations and Concomitant Phonon Anomalies in  $\text{Bi}_2\text{Sr}_2\text{LaCuO}_{6+\delta}$* , *Proc. Natl. Acad. Sci. U.S.A.* **117**, 16219 (2020).
- [43] Y. Shen, J. Sears, G. Fabbri, J. Li, J. Pellicciari, I. Jarrige, X. He, I. Božović, M. Mitrano, J. Zhang, J. F. Mitchell, A. S. Botana, V. Bisogni, M. R. Norman, S. Johnston, and M. P. M. Dean, *Role of Oxygen States in the Low Valence Nickelate  $\text{La}_4\text{Ni}_3\text{O}_8$* , *Phys. Rev. X* **12**, 011055 (2022).
- [44] A. J. Achkar, F. He, R. Sutarto, J. Geck, H. Zhang, Y.-J. Kim, and D. G. Hawthorn, *Resonant X-Ray Scattering Measurements of a Spatial Modulation of the Cu 3d and O 2p Energies in Stripe-Ordered Cuprate Superconductors*, *Phys. Rev. Lett.* **110**, 017001 (2013).
- [45] J. Q. Lin, P. Villar Arribi, G. Fabbri, A. S. Botana, D. Meyers, H. Miao, Y. Shen, D. G. Mazzone, J. Feng, S. G. Chiuzbăian *et al.*, *Strong Superexchange in a  $d^{9-\delta}$  Nickelate Revealed by Resonant Inelastic X-Ray Scattering*, *Phys. Rev. Lett.* **126**, 087001 (2021).
- [46] C. T. Chen, L. H. Tjeng, J. Kwo, H. L. Kao, P. Rudolf, F. Sette, and R. M. Fleming, *Out-of-Plane Orbital Characters of Intrinsic and Doped Holes in  $\text{La}_{2-x}\text{Sr}_x\text{CuO}_4$* , *Phys. Rev. Lett.* **68**, 2543 (1992).
- [47] M. Schneider, R. S. Unger, R. Mitdank, R. Müller, A. Krapf, S. Rogaschewski, H. Dwellk, C. Janowitz, and R. Manzke, *Evolution of the Density of States at the Fermi Level of  $\text{Bi}_{2-y}\text{Pb}_y\text{Sr}_{2-x}\text{La}_x\text{CuO}_{6+\delta}$  and  $\text{Bi}_2\text{Sr}_{2-x}\text{La}_x\text{CuO}_{6+\delta}$  Cuprates with Hole Doping*, *Phys. Rev. B* **72**, 014504 (2005).
- [48] F. C. Zhang and T. M. Rice, *Effective Hamiltonian for the Superconducting Cu Oxides*, *Phys. Rev. B* **37**, 3759 (1988).
- [49] M. Moretti Sala, V. Bisogni, C. Aruta, G. Balestrino, H. Berger, N. B. Brookes, G. M. d. Luca, D. Di Castro, M. Grioni, M. Guarise, P. G. Medaglia, F. Miletto Granozio, M. Minola, P. Perna, M. Radovic, M. Salluzzo, T. Schmitt, K. J. Zhou, L. Braicovich, and G. Ghiringhelli, *Energy and Symmetry of dd Excitations in Undoped Layered Cuprates Measured by Cu  $L_3$  Resonant Inelastic X-Ray Scattering*, *New J. Phys.* **13**, 043026 (2011).
- [50] H. Ulbrich, and M. Braden, *Neutron Scattering Studies on Stripe Phases in Non-Cuprate Materials*, *Physica (Amsterdam)* **481C**, 31 (2012).
- [51] A. Melikyan and M. R. Norman, *Symmetry of the Charge Density Wave in Cuprates*, *Phys. Rev. B* **89**, 024507 (2014).
- [52] P. Corboz, T. M. Rice, and M. Troyer, *Competing States in the t-J Model: Uniform d-Wave State versus Stripe State*, *Phys. Rev. Lett.* **113**, 046402 (2014).
- [53] H. Lu, M. Rossi, A. Nag, M. Osada, D. F. Li, K. Lee, B. Y. Wang, M. Garcia-Fernandez, S. Agrestini, Z. X. Shen, E. M. Been, B. Moritz, T. P. Devereaux, J. Zaanen, H. Y. Hwang, K.-J. Zhou, and W. S. Lee, *Magnetic Excitations in Infinite-Layer Nickelates*, *Science* **373**, 213 (2021).
- [54] D. Li, K. Lee, B. Y. Wang, M. Osada, S. Crossley, H. R. Lee, Y. Cui, Y. Hikita, and H. Y. Hwang, *Superconductivity in an Infinite-Layer Nickelate*, *Nature (London)* **572**, 624 (2019).
- [55] M. Osada, B. Y. Wang, B. H. Goodge, K. Lee, H. Yoon, K. Sakuma, D. Li, M. Miura, L. F. Kourkoutis, and H. Y. Hwang, *A Superconducting Praseodymium Nickelate with Infinite Layer Structure*, *Nano Lett.* **20**, 5735 (2020).
- [56] Low-valence nickelate electronic structures are rather similar provided they are compared at similar effective dopings [32,57].
- [57] H. LaBollita and A. S. Botana, *Electronic Structure and Magnetic Properties of Higher-Order Layered Nickelates:  $\text{La}_{n+1}\text{Ni}_n\text{O}_{2n+2}$  ( $n = 4-6$ )*, *Phys. Rev. B* **104**, 035148 (2021).
- [58] C. Schüßler-Langeheine, J. Schlappa, A. Tanaka, Z. Hu, C. F. Chang, E. Schierle, M. Benomar, H. Ott, E. Weschke, G. Kaindl, O. Friedt, G. A. Sawatzky, H.-J. Lin, C. T. Chen, M. Braden, and L. H. Tjeng, *Spectroscopy of Stripe Order in  $\text{La}_{1.8}\text{Sr}_{0.2}\text{NiO}_4$  Using Resonant Soft X-Ray Diffraction*, *Phys. Rev. Lett.* **95**, 156402 (2005).
- [59] EDRIXS, <https://github.com/NSLS-II/edrixs>, accessed May 19, 2022.
- [60] Y. Wang, G. Fabbri, M. Dean, and G. Kotliar, *EDRIXS: An Open Source Toolkit for Simulating Spectra of Resonant Inelastic X-Ray Scattering*, *Comput. Phys. Commun.* **243**, 151 (2019).
- [61] Y. Shen *et al.*, *Data Repository for: Electronic Character of Charge Order in Square Planar Low Valence Nickelates*, [10.5281/zenodo.7576428](https://zenodo.org/record/7576428) (2023).